A Solid-State Deuterium NMR Study of the Localized Dynamics at the C9pG10 Step in the DNA Dodecamer $[d(CGCGAATTCGCG)]_2$

Mary E. Hatcher,[†,§] Debra L. Mattiello,[†,||] Gary A. Meints,[†] John Orban,[‡] and Gary P. Drobny*[,†]

Contribution from the Department of Chemistry, University of Washington, Seattle, Washington 98195, and Center for Advanced Research in Biotechnology, University of Maryland, Biotechnology Institute, Rockville, Maryland 20850

Received April 21, 1997. Revised Manuscript Received December 31, 1997

Abstract: A solid-state deuterium NMR study of localized mobility at the C9pG10 step in the DNA dodecamer $[d(CGCGAATTCGCG)]_2$ is described. In contrast to the results of earlier deuterium NMR studies of furanose ring and backbone dynamics within the d(AATT) moiety, the furanose ring and helix backbone of dC9 display large amplitudes of motion on the 0.1 ms time scale at hydration levels characteristic of the B form structure. Solid-state deuterium NMR line shape data obtained from labeled dC9 DNA are interpreted using a composite motion model, in which the DNA oligomer is treated as rotating as a whole about the helix axis, while the base, furanose ring, and phosphodiester backbone execute localized motions. Consistent with past solid-state NMR studies, the amplitude and rate of the *uniform* rotation of the dC9-labeled oligomer are found to be sensitive to hydration level. Amplitudes of *localized* reorientational motions of C−D bonds in the furanose ring and backbone of dC9 are found to be larger than the librational amplitudes for the C−D bonds in the base of dC9, indicating that the pyrimidine base sugar does not move as a rigid entity and intersects a *locally* flexible region of the phosphodiester backbone. At hydration levels corresponding to 10−12 waters per nucleotide, Zeeman relaxation times for the furanose ring and backbone deuterons of dC9 in B form DNA equal 0.025 and 0.03 ms, respectively, and are the shortest relaxation times observed thus far for any deuteron in the DNA dodecamer at comparable hydration levels. The results of this solid-state NMR study suggest the existence of a significant dynamic component of sequence-specific recognition in this system.

1. Introduction

It has been long accepted that detailed structural information is necessary to fully understand the means by which duplex DNA interacts with transcription factors and, in general, performs the full range of its biological functions. Accordingly, our view of the structure of DNA has evolved through the years, as high-resolution structural models of DNA obtained by X-ray diffraction and solution NMR display sequence-specific variations from the canonical B form. It is reasonable to ask how an equally detailed picture of the internal dynamics of DNA would modify our view of these structural variations and thus our understanding of how DNA performs its biological functions.

In this paper we seek to further elucidate the internal, localized dynamics of DNA by exploring the mobility of a CpG step in the DNA dodecamer $[d(CGCGAATTCGCG)]_2$ using solid-state deuterium NMR. This DNA dodecamer contains the binding and cleavage site, d(GAATTC), for the EcoRI restriction endonuclease. The X-ray structure of this DNA dodecamer, crystallized in the B form, was published in 1981 by Dickerson and co-workers.[1] Since that time, various aspects of the structure have been investigated by X-ray crystallography,[2−5] solution-state NMR,[6−9] and molecular dynamics simulations.[10−16] X-ray data indicate that although the inner part of the restriction enzyme binding site d(GAATTC) has a structure similar to canonical B form, a number of sequence-specific structural variations occur throughout the dodecamer including variation of the sugar puckering between C3′-exo and O4′-endo, a slip of dT8 away from dC9, and a splay of the dC9-dG4 base pair. In addition, there occurs an overall bending of the helix by 19°.

† University of Washington.
‡ University of Maryland.
§ Current address: Department of Biochemistry, Brandeis University, 415 South Street, Waltham, MA 02254-9110.
|| Current address: Varian Associates, 3120 Hansen Way M/S D317, Palo Alto CA 94303.

(1) Drew, H. R.; Wing, R. M.; Takano, T.; Broka, C.; Tanaka, S.; Itakura, K.; Dickerson, R. E. *Proc. Nat. Acad. Sci. U.S.A.* **1981**, *78*, 2179−2183.
(2) Dickerson, R. E.; Drew, H. R. *J. Mol. Biol.* **1981**, *149*, 761−786.
(3) Drew, H. R.; Dickerson, R. E. *J. Mol. Biol.* **1981**, *151*, 535−556.
(4) Drew, H. R.; Samson, S.; Dickerson, R. E. *Proc. Nat. Acad. Sci. U.S.A.* **1982**, *79*, 4040−4044.
(5) Holbrook, S. R.; Dickerson, R. E.; Kim, S.-H. *Acta Crystallogr.* **1985**, *B41*, 255−262.
(6) Nerdal, W.; Hare, D. R.; Reid, B. R. *Biochemistry* **1989**, *28*, 1008.
(7) Zhu, L. In *Spin Dynamics Study and Structure Determination of Nucleic Acids by NMR*; Zhu, L., Ed.; University of Washington: Seattle, WA, 1994.
(8) Ott, J.; Eckstein, F. *Biochemistry* **1985**, *24*, 2530−2535.
(9) Bax, A.; Lerner, L. *J. Magn. Reson.* **1988**, *79*, 429−438.
(10) Kollman, P.; Keepers, J. W.; Weiner, P. *Biopolymers* **1982**, *21*, 2345−2376.
(11) McConnell, K. J.; Nirmala, R.; Young, M. A.; Ravishanker, G.; Beveridge, D. L. *J. Am. Chem. Soc.* **1994**, *116*, 4461−4462.
(12) Miaskiewicz, K.; Osman, R.; Weinstein, H. *J. Am. Chem. Soc.* **1993**, *115*, 1526−1537.
(13) Rao, S. N.; Kollman, P. *Biopolymers* **1990**, *29*, 517−532.
(14) Srinivasan, J.; Withka, J. M.; Beveridge, D. L. *Biophys. J.* **1990**, *58*, 533−547.
(15) Swaminathan, S.; Ravishanker, G.; Beveridge, D. L. *J. Am. Chem. Soc.* **1991**, *113*, 5027−5040.
(16) Withka, J. M.; Swaminathan, S.; Srinivasan, J.; Beveridge, D. L.; Bolton, P. H. *Science* **1992**, *255*, 597−599.

S0002-7863(97)01266-3 CCC: $15.00 © 1998 American Chemical Society
Published on Web 09/15/1998

It has been suggested that some of these structural modifications may constitute a significant component of sequence-specific recognition of the DNA binding site by the restriction enzyme.

The present study has a number of goals. First, as mentioned above, this paper seeks to further elucidate the local dynamics of the DNA dodecamer by investigating the internal motions of nucleotide dC9, which is located at a CpG step and is base-paired to dG4, the nucleotide located at the cleavage site. We will show that in contrast to the results derived by earlier ^{2}HNMR studies of nucleotides dA5, dA6, dT7, and dT8, the phosphodiester backbone, and the furanose sugar of dC9 display significant amplitudes of motion at rates on the order of 10^7 Hz. We will derive these dynamic rates and amplitudes from solid-state deuterium line shapes and relaxation data, and the results of our solid-state NMR study will be compared to the results of studies of the dynamics of the same region in [d(CGCGAATT**C**GCG)] $_2$ by solution-state NMR using proton scalar couplings,[9] and by a segmented rigid body analysis of X-ray diffraction data.[17] Finally, the origin of these localized, sequence-specific dynamics will be considered in the context of the local structure, and the role that these dynamics might play in sequence-specific protein−DNA recognition will be discussed.

2. Experimental Methods

A. Synthesis of Deuterated 2′-Deoxynucleosides and Phosphoramidites. [2′′-^{2}H]-2′-Deoxycytidine was prepared by the method of Robins et al.[18] with some minor modifications in solvents and purification procedures.[19] [5′/5′′-^{2}H]-2′-Deoxycytidine was prepared following the method of Orban and Reid[20] with only a modification in the starting material.

[5,6-^{2}H$_2$]-2′-Deoxycytidine was synthesized using the method of Maeda and Kawazoe[21] with some minor modifications.[22] Activated platinum was produced by slowly bubbling D_2 gas through a suspension of PtO_2 (Aldrich) in 30 mL of D_2O (Cambridge Isotopes). The suspension was allowed to settle and the liquid was pipetted away. Dry 2′-deoxycytidine (Aldrich, 681 mg, 3 mmol) and fresh D_2O were added to the reaction flask. D_2 gas was bubbled through the solution which was heated to 50 °C. Aliquots were periodically removed from the reaction vessel with a syringe, and the progress of the deuteration was monitored by high-resolution NMR. Deuteration at sites H5 and H6 was 95% complete after 45 h. The aqueous solution was filtered, lyophilized, and finally purified by recrystallization from a 95:5 EtOH/H_2O mixture. Lyophilization from deuterium-depleted water (Cambridge Isotopes) yielded 550 mg of [5,6-^{2}H]-2′-deoxycytidine.

2-(Cyanoethyl)-*N*,*N*-diisopropylaminophosphoramidites were synthesized as described in Huang et al.,[26] using the procedure of Ti et al.[23] to convert deuterated 2′-deoxycytidine to 5′-O-(dimethoxytrityl)-6-*N*-benzoyl-2′-deoxycytidine and the procedures of Barone et al.[24] and Sinha et al.[25] to produce 5′-O-(dimethoxytrityl)-6-*N*-benzoyl-2′-deoxycytidine-3′-(2-(cyanoethyl)-*N*,*N*′-diisopropylamino)phosphoramidite.

B. DNA Synthesis and Purification. Selectively deuterated 2′-deoxycytidine phosphoramidites were incorporated into the DNA sequence [d(CGCGAATTCGCG)$_2$] at the C9 position using an Applied Biosystems 392 DNA/RNA synthesizer. The resulting oligonucleotides were deprotected in aqueous ammonia before purification. The DNA oligonucleotides were purified by ethanol precipitation and then loaded on a G-25 Sephadex column (Pharmacia). The fractions were monitored by UV spectroscopy at $\lambda = 260$ nm and analyzed via polyacrylamide gel electrophoresis. The appropriate fractions were then pooled, salted to 10 wt % with NaCl, and subjected to repeated lyophilization from deuterium-depleted water to remove any D_2O present. The samples were packed into 5 mm solid-state NMR Kel-F sample holders and again lyophilized. Hydration of the DNA samples was achieved by vapor diffusion in controlled humidity chambers. These chambers contain saturated salt solutions (in deuterium-depleted water) of known relative humidity.[26] In this paper, hydration level is quantified by the parameter *W*, the number of water molecules bound per nucleotide.

C. Solid-State Deuterium NMR Spectroscopy. An extremely important aspect of solid-state deuterium NMR is its ability to probe motions with correlation times ranging over 10 orders of magnitude.[27,28] In the fast exchange limit, $\tau_c < 10^{-7}$ s, the line shape can be parametrized by "preaveraged" tensor parameters: QCC_{eff}, the effective quadrupolar coupling constant, and η_{eff}, the effective asymmetry parameter. Within this motional regime the deuterium resonant frequency is given by eq 1:

$$\omega_Q = \pm\frac{3\pi}{4}\left(\frac{e^2qQ}{h}\right)_{\text{eff}}[3\cos^2\Theta - 1 + \eta_{\text{eff}}\sin^2\Theta\cos 2\Phi] \quad (1)$$

To obtain an expression for QCC_{eff}, the orientationally averaged EFG tensor $\bar{V}_{kl}$ is first calculated using the equilibrium distribution function $P(\Omega)$. For discrete jump processes

$$\bar{V}_{kl} = \sum_j P(\Omega_j)\bar{V}_{kl}P(\Omega_j) \quad (2a)$$

where

$$V(\Omega_j) = -\frac{eq}{2}\begin{pmatrix} 1-3\cos^2\phi_j\sin^2\theta_j & {}^3/_2\sin 2\phi_j\sin^2\theta_j & {}^3/_2\cos\phi_j\sin 2\theta_j \\ {}^3/_2\sin 2\phi_j\sin^2\theta_j & 1-\sin^2\phi_j\sin^2\theta_j & -{}^3/_2\sin\phi_j\sin 2\theta_j \\ {}^3/_2\cos\phi_j\sin 2\theta_j & -{}^3/_2\sin\phi_j\sin 2\theta_j & 1-3\cos^2\theta_j \end{pmatrix} \quad (2b)$$

In the case that the EFG tensor is axially symmetric, the polar and azimuthal angles θ_j and θ_j, respectively, are used to orient the principal axis system of the EFG tensor at the *i*th jump site in the LAB frame. QCC_{eff} is finally calculated by determining the eigenvalues of the averaged EFG tensor. Considering only the axial component ($\eta = 0$), using the conventions of Torchia and Szabo[29] and first-order perturbation theory, the resonant frequency for an *N*-site jump process is given by

$$\omega_Q = \pm\frac{3e^2qQ}{4\hbar}\sum_{j=1}^{N} p_j^{\text{eq}}\sum_{a=-2}^{+2} d_{0d}^{(2)}(\theta)\, d_{0d}^{(2)}(\theta_j)\cos[a(\theta_j - \Phi)] \quad (3)$$

The formulation summarized in eqs 3−6 is not general enough to treat the case in which the rate of molecular motion is arbitrary compared to the deuterium quadrupolar frequency ω_Q. In general, the rotating frame equations of motion for the transverse components of the magnetization $M(\theta,\Phi)$ are modified to include the dynamic process

(17) Holbrook, S. R.; Kim, S.-H. *J. Mol. Biol.* **1984**, *173*, 361−388.
(18) Robins, M. J.; Wilson, J. S.; Hansske, F. *J. Am. Chem. Soc.* **1983**, *105*, 4059−4065.
(19) Huang, W.-C.; Orban, J.; Kintanar, A.; Reid, B. R.; Drobny, G. P. *J. Am. Chem. Soc.* **1990**, *112*, 9059−9068.
(20) Orban, J.; Reid, B. R. *J. Labeled Compd. Radiopharm.* **1989**, *27*, 195−198.
(21) Maeda, M.; Kawazoe, Y. *Tetra. Lett.* **1975**, *19*, 1643−1646.
(22) Mattiello, D. L. In *Investigation of Zeeman and Quadrupolar Relaxation to Elucidate Furanose Ring Dynamics in Synthetic Oligonucleotides*; Mattiello, D. L., Ed.; University of Washington: Seattle, WA, 1993.
(23) Ti, G. S.; Gaffney, B. L.; Jones, R. A. *J. Am. Chem. Soc.* **1983**, *104*, 1316.
(24) Barone, A. D.; Tang, J.-Y.; Caruthers, M. H. *Nucleic Acids Res.* **1984**, *12*, 409.
(25) Sinha, N. D.; Biernat, J.; McManus, J.; Koster, H. *Nucleic Acids Res.* **1984**, *12*, 4539−4557.
(26) *CRC Handbook of Chemistry and Physics*; Weast, R. C., Ed.; CRC: Boca Raton, FL, 1979; p E-46.
(27) Abragam, A. *Principles of Nuclear Magnetism*; Oxford University Press: New York, 1961.
(28) Spiess, H. W. In *Dynamic NMR Spectroscopy*; Spiess, H. W., Ed.; Springer-Verlag: New York, 1978; Vol. 15, pp 56−214.
(29) Torchia, D. A.; Szabo, A. *J. Magn. Reson.* **1982**, *49*, 107−121.

$$\dot{M}_{\pm}(\theta,\Phi) = [i\omega_{\pm}(\theta,\Phi) + R(\theta,\Phi)]M_{\pm}(\theta,\Phi) \quad (4)$$

where $M_{\pm}(\theta,\Phi) = M_X(\theta,\Phi) \pm iM_y(\theta,\Phi)$. For the case of continuous dynamics, $R(\theta,\Phi)$ is the diffusion operator. For discrete jump dynamics, $R(\theta,\Phi)$ is represented by the jump matrix, in which case eq 4 assumes the form

$$\dot{M}_{\pm} = \sum_{j=1}^{N}(i\omega_{\pm,i}\delta_{ij} + R_{ij})M_{\pm,j} \quad (4')$$

The off-diagonal elements R_{ij} must satisfy microscopic reversibilty, i.e., $R_{ij}P_j = R_{ji}P_i$, where P_i is the a priori population of the ith site. The diagonal elements R_{ii} must be the negative of the sum of the elements in the ith row. To probe for dynamic processes with rates occurring in the intermediate (10^{-7} s $\leq \tau_c \leq 10^{-5}$ s) and slow motion regimes (10^{-5} s $\leq \tau_c \leq 10^{-4}$ s), the deuterium solid-state line shape is calculated by numerically integrating eq 4.′

All ^{2}H NMR experiments described in this paper were performed on a home-built NMR spectrometer operating at a deuterium Larmor frequency of 76.76 MHz (Gladden and Drobny, unpublished results). An ENI LPI-10 radio frequency amplifier was used to generate the high power pulsed radio frequency irradiations (90° pulse times = 2.3−3.0 μs) required to excite the entire spectral width (200 kHz) of the deuterated DNA samples.

The deuterium NMR spectrum was acquired using a quadrupole echo pulse sequence with an eight-step phase cycling regime.[39] The delay between pulses was typically 40 μs, and the dwell time was 200 ns. Data acquisition was initiated prior to the echo maximum so the time domain data were left-shifted prior to Fourier transformation. The spectra were apodized with 1000−5000 Hz Lorentzian line broadening. Quadrupolar echo line shapes were calculated using the program MXQET.[40] Partially recovered line shapes were simulated using the program MXET1.[41]

The spin−lattice relaxation time, T_{1Z}, was determined using an inversion recovery (IR) pulse sequence, which incorporated a 180° composite pulse to ensure broadband inversion.[22,42] To obtain a powder-averaged spin−lattice relaxation time $\langle T_{1Z}\rangle$, the integrated intensity of the powder pattern was monitored as a function of recovery time. The quadrupolar relaxation time $\langle T_{1Q}\rangle$ was determined using the Jeener−Broekaert pulse sequence[36,37] to create quadrupolar order, by varying the length τ_2 of the evolution period to monitor the decay of the spin alignment echo amplitude. To ensure preparation of quadrupolar order over a broad spectral band width, a composite pulse sequence[43] was substituted for the 90x pulse in the basic Jeener−Broekaert pulse sequence. The period τ_1 was set to 40 μs. Data from these relaxation experiments were analyzed using a nonlinear least-squares fitting routine.[44]

3. Results

Solid-state deuterium line shape and relaxation data are presented for each isotopically labeled site of the nucleoside dC9. These sites include positions on the cytosine base (H5 and H6), the furanose ring (H2″), and the backbone methylene group (H5′/5″). Experimental line shape and relaxation data displayed in the results section are accompanied by a brief discussion of the dynamics at a qualitative level. Numerical simulations of solid-state deuterium line shapes and other quantitative estimates of dynamic amplitudes and rates are presented in section 4. A comparison of the results of the current study with structural models for DNA derived by X-ray diffraction and NMR are presented in section 5.

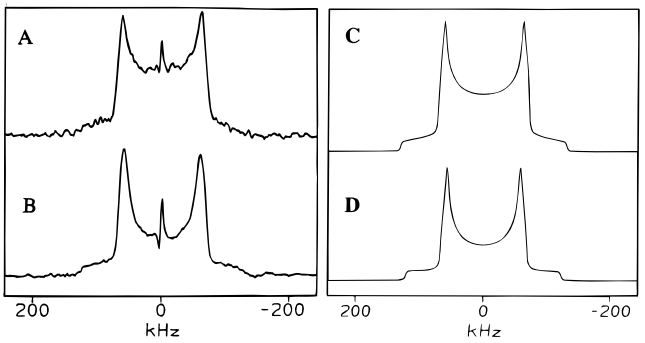

Figure 1. Experimental and simulated solid-state deuterium line shapes for [d(CGCGAATTC*GCG)]$_2$ labeled with [5,6-^{2}H$_2$]-2′-deoxycytidine. (A) Experimental deuterium line shape observed for the deuterons D5 and D6 on the base of dC9 for $W \approx 0$ (i.e., lyophilized). (B) Deuterium solid-state NMR line shape for the same sample as in part A at W = 10.1. (C) Simulated $W \approx 0$ spectrum. $QCC_{eff} = 17 \pm 22$ kHz; $\eta_{eff} = 0.060 \pm 0.1$. The small reduction of the quadrupolar coupling constant can be simulated by a libration of the base by 6° for which $k = 10^6$ Hz. (D) Simulated $W = 10.1$ spectrum. The dynamic model assumes a composite motion. A localized motion about an axis perpendicular to the helix axis with slightly increased amplitude (9°) accounts for the continued decrease in QCC_{eff}, and a slow rotation about the helix axis ($N = 6$, $\Phi_{ij} = 30°$, $k_{helix} = 10^4$ Hz) accounts for the decrease in the line shape intensity.

A. Base Dynamics. [5,6-^{2}H]-2′-Deoxycytidine Incorporated at dC9. Solid-state ^{2}H NMR line shapes of [5,6-^{2}H]-2′-deoxycytidine, incorporated at the dC9 position of the DNA dodecamer [d(CGCGAATT**C**GCG)]$_2$,were studied at four hydration levels corresponding to $W \approx 0$ (i.e., lyophilized material), $W = 10.1$, 13.2, and 16.2. Experimental line shapes, shown in Figure 1, are parametrized by an effective quadrupolar coupling constant (QCC_{eff}) and an effective asymmetry parameter (η_{eff}). The deuterium NMR line shape versus W is dominated by two trends. First, no significant decrease in the breadth of the powder pattern occurs as a function of hydration level W. The effective quadrupolar coupling constant (QCC_{eff}) decreases only slightly from 172 ± 2 to 168 ± 2 kHz over the hydration range of $W = 0-16$, and the effective asymmetry η_{eff} remains constant at 0.060 ± 0.01. Second, spectral intensity decreases with increasing hydration, especially in the center of the spectrum. These same line shape trends have been observed over comparable hydration ranges for the same DNA dodecamer deuterated at all purine H8 positions [d(CG*CG*A*A*TTCG*CG*)]$_2$ and selectively deuterated at the H6 position of T7 [d(CGCGAAT*TCGCG)]$_2$.[45]

The fact that the overall spectral width is undiminished as W increases indicates that there is no large amplitude motion of the base on a time scale fast compared to time scale of the quadrupolar interaction ($\tau_c < 10^{-7}$ s). The dramatic reduction in signal intensity is undoubtedly due to slow motion that occurs on a time scale comparable to the time scale required for

(30) Alam, T. M.; Drobny, G. P. *Chem. Rev.* **1991**, *91*, 1545−1590.
(31) Alam, T. M.; Orban, J.; Drobny, G. P. *Biochemistry* **1990**, *29*, 9610−9617.
(32) Alam, T. M.; Orban, J.; Drobny, G. P. *Biochemistry* **1991**, *30*, 9229−9237.
(33) Brandes, R.; Vold, R. R.; Vold, R. L.; Kearns, D. R. *Biochemistry* **1986**, *25*, 7744−7751.
(34) Brandes, R.; Vold, R. R.; Kearns, D. R.; Rupprecht, A. *Biochemistry* **1990**, *29*, 1717−1721.
(35) Nuutero, S.; Fujimoto, B. S.; Flynn, P. F.; Reid, B. R.; Ribeiro, N. S.; Schurr, J. M. *Biopolymers* **1994**, *34*, 463−480.
(36) Jeener, J.; Broekaert, P. *Phys. Rev.* **1967**, *157*, 232.
(37) Lausch, M.; Spiess, H. W. *J. Magn. Reson.* **1983**, *54*, 466−479.
(38) Spiess, H. W.; Sillescu, H. *J. Magn. Reson.* **1981**, *42*, 381−389.
(39) Griffin, R. G. *Methods Enzymol.* **1981**, *72*, 108−174.
(40) Greenfield, M. S.; Ronemus, A. D.; Vold, R. L.; Ellis, P. D.; Raidy, T. E. *J. Magn. Reson.* **1987**, *72*, 89.
(41) Vold, R. R.; Vold, R. L. *Adv. Magn. Opt. Reson.* **1991**, *16*, 85−171.
(42) Tycko, R. *Phys. Rev. Lett.* **1983**, *51*, 775.
(43) Wimperis, S. J. *J. Magn. Reson.* **1990**, *86*, 46.
(44) DeFontaine, D. L.; Ross, D. L.; Ternai, B. *J. Magn. Reson.* **1975**, *18*, 276−281.
(45) Kintanar, A.; Huang, W.-C.; Schindele, D. C.; Wemmer, D. E.; Drobny, G. P. *Biochemistry* **1989**, *28*, 282−293.

Table 1. Line Shape and Relaxation Parametersfor [5,6-^{2}H]-2′-Deoxycytidine in d[CGCGAATTC*GCG]$_2$

RH	dry	75	88
W^a	0	10.1	16.2
QCC_{eff} (kHz)	172 ± 2	168 ± 2	168 ± 2
η_{eff}	0.06 ± 0.01	0.06 ± 0.01	0.06 ± 0.01
$\langle T_{1Z}\rangle$ (s)	6.00 ± 0.80	0.10 ± 0.015	0.060 ± 0.01
$\langle T_{1Q}\rangle$ (s)	*b*	0.082 ± 0.012	0.036 ± 0.01

[a] mol of H_2O/mol of nucleotide. [b] Quantity not measured or determined.

formation of the quadrupolar echo.[38] In such a scenario, an internal motion changes the orientation of the EFG tensor of a deuteron relative to the magnetic field direction on the time scale of the quadrupolar echo pulse sequence ($\tau_c = 10^{-6}-10^{-4}$ s). The frequency of echo dephasing would be different from the frequency of echo rephasing, diminishing the intensity of the echo. Isochromats precessing at frequencies on the order of the dynamics or slower would be most affected, hence the loss of intensity near the center of the spectrum. A summary of QCC_{eff}, η_{eff}, and relaxation data for this sample is given in Table 1.

The powder-averaged spin−lattice relaxation time $\langle T_{1Z}\rangle$ for this sample in the dry, lyophilized state is 6 s. $\langle T_{1Z}\rangle$ decreases to 0.100 ± 0.015 s at $W = 10.1$ and to 0.060 ± 0.010 s at $W = 16.2$. In Figure 2A, the complete inversion−recovery line shape series is shown for $W = 10.1$. Quadrupolar echo decay data are also shown for $W = 10.1$ in Figure 2B. At $W = 10.1$, the powder-averaged quadrupolar relaxation time $\langle T_{1Q}\rangle$ was found to be 0.0820 ± 0.012 s, and at $W = 16.2$, $\langle T_{1Q}\rangle = 0.0360$ ± 0.01 s.

B. Furanose Ring Dynamics. [2″-^{2}H]-2′-Deoxycytidine Incorporated at dC9. To probe furanose ring dynamics at dC9, solid-state deuterium NMR line shapes and relaxation data were obtained for [2″-^{2}H]-2′-deoxycytidine-labeled [d(CGCGAATTCGCG)]$_2$ at nine hydration levels ranging from the lyophilized ($W \approx 0$) state to $W = 22.2$. The solid-state deuterium line shape, recorded as a function of hydration level for $W = 0$, 12.3, and 22.2 are displayed at the left in Figure 3. Line shape data for the complete series of hydration levels taken at room temperature are shown in Table 2. For hydration levels within the range of $W = 0-5.5$, the deuterium solid-state NMR line shape is typified by the data in Figure 3A: a Pake doublet powder pattern displaying some minor averaging, perhaps resulting from restricted motions in the fast rate limit. For the hydration regime $W = 0-5.5$, QCC_{eff} decreases from 170 ± 2 kHz at $W \approx 0$ to 166 ± 2 kHz at $W = 5.5$. The effective asymmetry parameter varies from 0.020 ± 0.1 at $W = 0.0$ to 0.040 ± 0.1 at $W = 5.5$.

For the hydration range of $W = 12.3-15.2$, deuterium line shapes display features characteristic of extensive averaging at intermediate rates (Figure 3B) and thus cannot be described by effective tensor parameters QCC_{eff} and η_{eff}. However, in the hydration range of $W = 16.8-22.2$, line shapes characteristic of fast regime averaging reappear but with greatly diminished QCC_{eff} values. Specifically, QCC_{eff} decreases from 78 ± 2 kHz at $W = 16.8$ to 60 ± 2 kHz at $W = 22.2$ (Figure 3C). The transition in deuterium line shape for the 2″ deuteron of dC9 from an essentially rigid powder pattern at low hydration levels $W < 12.3$, passing through an intermediately averaged pattern in the hydration range of $W = 12.3-15.5$, and emerging as a motionally narrowed powder pattern at high hydration levels, i.e., $W > 15.5$, is in contrast to the behavior observed over the same hydration range for the same dodecamer 2″-deuterated at the dA5 and dA6 nucleotides.[19] The deuterium line shapes observed at those sites display a trend as a function of hydration

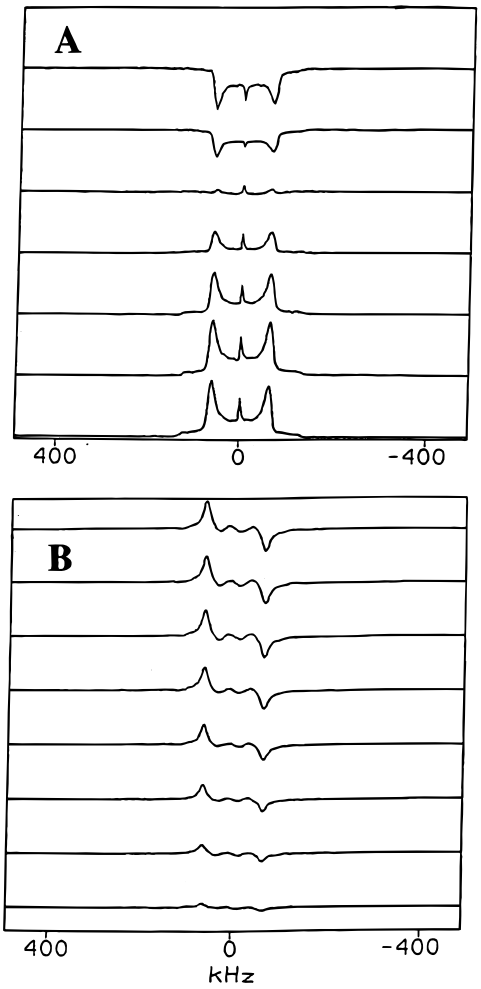

Figure 2. Deuterium solid-state NMR line shapes observed at $W = 13$ for [d(CGCGAATTC*GCG)]$_2$ labeled with [5,6-$^2H_2$]-2′-deoxycytidine. (A) Partially recovered line shapes acquired after an inversion−recovery pulse sequence. Delay times are, from top to bottom, (in milliseconds): 1, 10, 50, 100, 200, 400, 500. (B) Spectra obtained by Fourier transformation of the spin alignment echo following a Jeener−Broekaert pulse sequence and plotted as a function of evolution time τ_2 for 0.5, 1.0, 5.0, 10, 25, 50, 100, and 200 ms.

essentially identical to base-deuterated dodecamers: the width of the deuterium powder pattern is undiminished as W increases, but the overall intensity of the powder pattern decreases at high hydration levels.

$\langle T_{1Z}\rangle$ for the 2″ deuteron of dC9 was measured at room temperature at nine hydration levels between $W = 0$ and 22.2. In Figure 4A, a complete inversion−recovery data set for the 2″ deuteron of dC9 at $W = 12.3$ is displayed, and the powder-averaged Zeeman relaxation time $\langle T_{1Z}\rangle$ for the 2″ deuteron of dC9 is displayed in Figure 5A as a function of W along with similar data for other deuterons in the DNA dodecamer. The spin lattice relaxation of the 5/6 deuterons on the dC9 base shows the familiar trend over the hydration range of $W = 0-16.2$ that has been observed in other base-deuterated DNA oligomers and high molecular weight DNA: $\langle T_{1Z}\rangle$ gradually decreases from a maximum of 6.00 s at $W = 0$ to a minimum of 0.06 s at $W = 16.3$.[33,34,45] A similar trend is observed for the 2″ deuterons of dA5 and dA6.[19] The behavior of $\langle T_{1Z}\rangle$ for the 2″ deuteron of dC9 over the same hydration range shows a rapid decrease from a maximum of 1.8 s at $W = 0$, to 0.02 s at $W = 12.3$. At $W = 12.3$, T_{1Z} varied slightly across the powder pattern, increasing from less than 0.02 s at frequencies less than 25 kHz to about 0.028 s near the edges of the powder pattern.

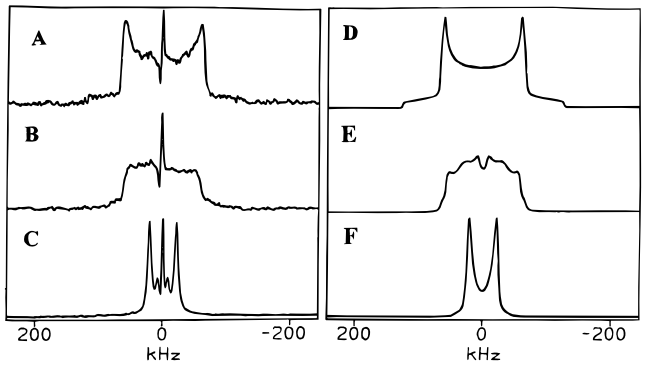

Figure 3. Experimental and simulated solid-state deuterium line shapes for [d(CGCGAATTC*GCG)]$_2$ labeled with [2″-^{2}H]-2′-deoxycytidine. (A) Solid-state deuterium NMR line shape observed at a hydration level of $W = 5.5$. (B) Deuterium line shape observed at a hydration level of $W = 12.3$. (C) Deuterium line shape observed at $W = 22.2$. (D) Simulated deuterium line shape for $W = 5.5$ data. The reduction in the quadrupolar coupling constant can be produced by a small amplitude libration (8°) at a rate $k = 10^7$ Hz. (E) Simulated deuterium line shape for $W = 12.3$ data. A composite motion model is used to simulate the data. The localized motion is assumed to be a two site exchange for which the amplitude is 38 degrees and $k = 10^7$ Hz. Axes are chosen so the C−D bond vector makes an angle of about 20° with the helix axis (i.e., C2′-endo). The second, slower motion is assumed to be around the helix axis ($N = 6$, $\Phi_{ij} = 20°$, $k = 10^4$ Hz). (F) Simulated $W = 22.2$ data. A composite motion model is again used with almost the same parameters for the localized motion of the furanose ring ($N = 2$, $\Phi = 40°$, $k = 10^7$ Hz). The helix axis motion is assumed to occur at a higher rate than for the $W = 12.3$ data ($N = 6$, $\Phi_{ij} = 60°$, $k = 5 \times 10^6$ Hz). On the basis of earlier studies of DNA dodecamers at high hydration levels, cholesteric ordering is assumed (see text for details).

At $W = 12.3$, the rate of spin lattice relaxation of the 2″ deuteron of dC9 is the highest for any deuteron in this DNA dodecamer at comparable hydration level. For example, at $W = 12.3$, $\langle T_{1Z}\rangle$ for the 2″ deuteron of dC9 is about 10% of the $\langle T_{1Z}\rangle$ for the dA5/6 2″ deuterons. From $W = 12.3$ to 22.2, $\langle T_{1Z}\rangle$ decreases only slightly from 0.020 to 0.015 s We conclude that whatever motion is responsible for the relaxation of the 2″ deuteron of dC9, it is comparatively efficient, and its efficiency dramatically increases between $W = 5.5$ and $W = 12.3$. The Zeeman relaxation of the 2″ deuteron of dC9 versus W is discussed further in section 4.

The quadrupolar relaxation time $\langle T_{1Q}\rangle$ was determined to be 0.025 s at $W = 12.3$. To within experimental error, $\langle T_{1Q}\rangle$ was the same at $W = 13.6$ and 15.2. There was no significant variation in T_{1Q} over the range of frequencies within the powder pattern. Figure 4B shows the deuterium line shape following a Jeener−Broekaert pulse sequence for $W = 12.3$, and Figure 5B compares the decay of the spin alignment echo for the 2″ deuteron of dC9 at $W = 12.3$ to the decay of the spin alignment echo for the 5/6 deuterons of the base of dC9 at a comparable hydration level. Figures 5A and B both demonstrate that the rates of decay of both Zeeman and quadrupolar order are significantly different for the base versus the ribose ring of dC9. Decay of the spin alignment echo amplitude has been studied by Hiyama et al. for furanose-deuterated thymidine monomer,[46] and interpreted by those authors in terms of a slow repuckering of the deoxyribose ring using a two-site jump model of sugar ring dynamics and a correlation time of 1 ms.

C. Backbone Dynamics. [5′/5″-^{2}H$_2$]-2′-Deoxycytidine Incorporated at dC9. Backbone dynamics in the [5′/5″-^{2}H$_2$]-2′-deoxythymidine-labeled DNA dodecamer [d(CGCGAAT*T*CGCG)]$_2$ have been studied previously by solid-state deuterium NMR.[32] It was found that over the hydration range of $W = 0.0-20.5$, the effective quadrupolar coupling constant QCC_{eff} decreases from 164 to 143 kHz. The spin lattice relaxation time $\langle T_{1Z}\rangle$ decreases from 0.5 s at $W = 0.0$ to 0.040 s at $W = 16.3$, and $\langle T_{2e}\rangle$ decreases from 0.165 s to 0.040 s over the same range of hydration levels. The latter value is very short in comparison to $\langle T_{2e}\rangle$ values for base and furanose deuterons at dT7/8 and at other sites on the DNA dodecamer at comparable levels of hydration. At $W = 16.3$, the intensity of the quadrupolar echo of the 5′/5″ deuterons of dT7/8 is greatly diminished. The variation in line shape and spin lattice relaxation rate over the hydration range of $W = 0.0-25.2$ was analyzed using the same models of helix motion used to treat the deuterium NMR data acquired from base-deuterated[45] and furanose-deuterated[19] DNA oligomers. In addition the fast, localized motion of the backbone at dT7 and dT8 was modeled as a four-site libration characterized by two amplitudes θ_0 and ϕ_0. The root-mean-square amplitude $\mathrm{rms}(\theta_0, \phi_0) = \sqrt{(\theta_0+\phi_0)/2}$ increased slightly with hydration to a maximum of $21 \pm 2°$ at $W = 16.3$, which is only 4−5° greater than the dynamic amplitudes of the 2″ deuterons on the furanose rings of dT7 and dT8 at comparable hydration levels.[47]

Deuterium NMR line shape and relaxation data indicate that the dynamics of the backbone of dC9 differ greatly from the backbone dynamics at dT7 and dT8. The deuterium line shape for the DNA dodecamer [d(CGCGAATTC*GCG)]$_2$, labeled with [5′/5″-^{2}H$_2$]-2′-deoxycytidine at dC9, was studied in detail at only a single hydration level, $W = 10.5$, because, even at this low a hydration level, $\langle T_{2e}\rangle \approx 0.04$ s and the amplitude of the quadrupolar echo was greatly diminished. Figure 6A shows the deuterium powder pattern obtained for about 25−30 mg of the DNA dodecamer deuterated at the 5′/5″ position of dC9. For comparison, Figure 6B shows the spectrum of the same DNA dodecamer with [2″-^{2}H]-2′-deoxycytidine incorporated at dC9 at $W = 10-11$, and Figure 6C is the same DNA dodecamer deuterated at the base of dC9 and hydrated to $W = 10-11$. Despite the low signal-to-noise of the data in Figure 6A, the spectrum clearly is a motionally narrowed powder pattern with a $QCC_{eff} \approx 60$ kHz, indicating that the backbone methylene group at dC9, like the furanose, is extremely mobile even at relatively low levels of hydration. $\langle T_{1Z}\rangle$ of the dC9 backbone-labeled sample at $W = 10.5$ was found to be 30 ± 10 ms, which is shorter than the spin lattice relaxation time observed for the 5′/5″ deuterons of dT7 and dT8 even at high levels of hydration, i.e., $W > 16$. The small sample size and low sensitivity did not allow a measurement of $\langle T_{1Q}\rangle$ at this hydration level. At hydration levels $W > 20$, a single motionally narrowed line was observed (data not shown), again in contrast to the data from the 5′/5″ deuterons of dT7 and dT8.

4. Calculations

A fundamental challenge underlying any analysis of the NMR line shape of DNA is to deconvolute the effect of motions of the oligomer as a whole from the effects of localized motions that are associated with single structural entities such as individual bases, furanose rings, or phosphodiester groups. To address this problem, we assume that at low hydration levels the overall motion of the DNA dodecamer can be portrayed as the motion of a rigid rod. Specifically, we assume, for the

(46) Hiyama, Y.; Roy, S.; Cohen, J. S.; Torchia, D. A. *J. Am. Chem. Soc.* **1989**, *111*, 8609−8613.

(47) Hatcher, M. E. In *A Solid State Deuterium NMR Investigation of the Local Dynamics of Nucleotides in the EcoRI Restriction Endonuclease Binding Site*; Hatcher, M. E., Ed.; University of Washington: Seattle, WA, 1996.

Table 2. Line Shape and Relaxation Parametersfor [2″-^{2}H]-2′-Deoxycytidine in d[CGCGAATTC*GCG]$_2$

RH	dry	33	66	75	80	84	88	90	93
W^a	0	3.3	5.5	12.3	13.6	15.2	16.8	18.4	22.2
QCC_{eff} (kHz)	170 ± 2	168 ± 2	166 ± 2	*b*	*b*	*b*	78 ± 2	76 ± 2	60 ± 2
η_{eff}	0.02 ± 0.01	0.02 ± 0.01	0.04 ± 0.01	*b*	*b*	*b*	0.04 ± 0.01	0.04 ± 0.01	0.02 ± 0.01
$\langle T_{1Z}\rangle$ (s)	1.80 ± 0.27	0.65 ± 0.15	0.18 ± 0.05	0.20 ± 0.010	0.020 ± 0.01	0.016 ± 0.010	0.020 ± 0.010	0.014 ± 0.010	0.015 ± 0.010
$\langle T_{1Q}\rangle$ (s)	*c*	*c*	*c*	*c*	*c*	0.026 ± 0.010	*c*	*c*	0.025 ± 0.010

[a] mol of H_2O/mol of nucleotide. [b] Intermediate rate line shape. [c] Quantity not measured or determined.

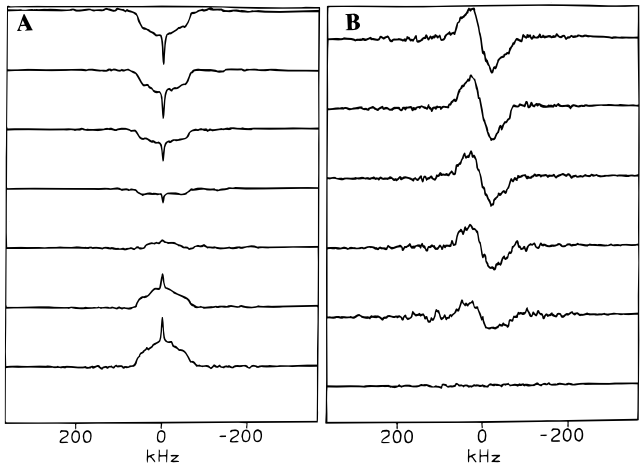

Figure 4. Deuterium solid-state NMR line shapes observed at $W = 12.3$ for [d(CGCGAATTC*GCG)]$_2$ labeled with [2″-^{2}H]-2′-deoxycytidine. (A) Partially recovered line shapes acquired after an inversion−recovery pulse sequence. Delay times are, from top to bottom, (in milliseconds): 1, 10, 50, 100, 200, 400, 500. (B) Deuterium line shapes acquired followong a Jeener−Broekaert pulse sequence. Evolutions times τ_2 are, from top to bottom, (in milliseconds): 0.5, 1, 5, 10, 25, 100.

purpose of simulating solid-state deuterium line shapes, that the uniform motion of solid dodecameric DNA in the hydration range of $W = 0-22$ can be described as a restricted diffusion of the whole oligomer about the helix axis at a rate and amplitude that vary with hydration level *W*. These uniform motion parameters are not, however, treated as freely adjustable quantities in the present study, but are confined to a narrow range of values derived in a number of independent studies of selectively deuterated DNA dodecamers.[30] In earlier DNA studies, restricted diffusion about the helix axis was approximated as a discrete jump process between nearest neighbor sites with equal site probabilities, i.e., eq 5,

$$S_1 \underset{}{\overset{k}{\rightleftarrows}} S_2 \overset{k}{\rightleftarrows} \cdots \overset{k}{\rightleftarrows} S_n \qquad (5)$$

where the relationship between the diffusion coeffcient *D*, the kinetic constant *k*, and the jump correlation time τ_c is given by

$$D \approx \frac{k\phi_{ij}^2}{2} = \frac{\phi_{ij}^2}{\tau_c} \qquad (6)$$

where ϕ_{ij} is the half-arc angle between successive sites *i* and *j*. As the number of sites *N* increases or as the size of ϕ_{ij} decreases, the limit of true diffusion is approached. In practice, deuterium line shapes for DNA do not vary markedly for N ≥ 6. Therefore, as in earlier solid-state NMR studies of deuterated, dodecameric DNA, uniform motion of the oligomer will be simulated at most as a 6-fold ($N = 6$) jump between nearest neighbor sites where D_R (i.e., *k* and ϕ_{ij}) varies with *W*. Given this assumption, the general approach is to test various models

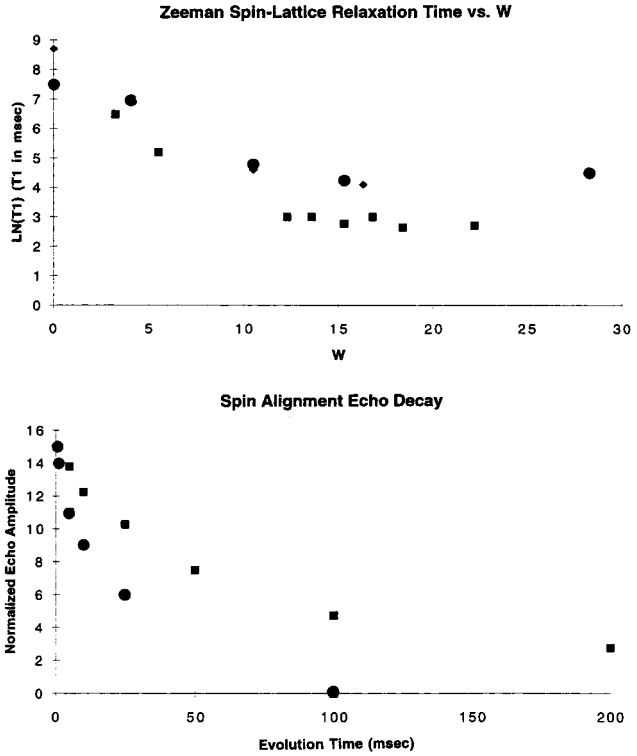

Figure 5. (A) Plots of $\langle T_{1Z}\rangle$ versus *W* for [d(CGCGAATTC*GCG)]$_2$ labeled with [2″-^{2}H]-2′-deoxycytidine (■), [5,6-$^2H_2$]-2′-deoxycytidine (◆), and for [d(CGCGA*A*TTCGCG)]$_2$ labeled with [2″-^{2}H]-2′-deoxyadenosine (●). (B) Plots of spin alignment echo amplitude versus τ_2 for [d(CGCGAATTC*GCG)]$_2$ labeled with [2″-^{2}H]-2′-deoxycytidine (●) and [5,6-$^2H_2$]-2′-deoxycytidine (■) at $W = 10-12.3$.

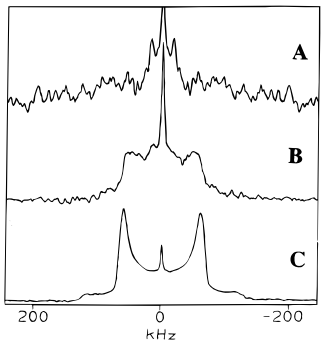

Figure 6. Quadrupolar echo spectra obtained for DNA dodecamers deuterated on the base, sugar ring, and backbone of the dC9 nucleotide. (A) Quadrupolar echo spectrum of [d(CGCGAATTC*GCG)]$_2$ labeled with [5′/5″-^{2}H]-2′-deoxycytidine and hydrated to $W = 10.1$. (B) Quadrupolar echo spectrum of [d(CGCGAATTC*GCG)]$_2$ labeled with [2″-^{2}H]-2′-deoxycytidine and hydrated to $W = 10-11$. (C) Quadrupolar echo spectrum of [d(CGCGAATTC*GCG)]$_2$ labeled with [5,6-$^2H_2$]-2′-deoxycytidine and hydrated to $W = 10-11$.

of the localized motion of various nucleotide components against the deuterium data presented in section 3.

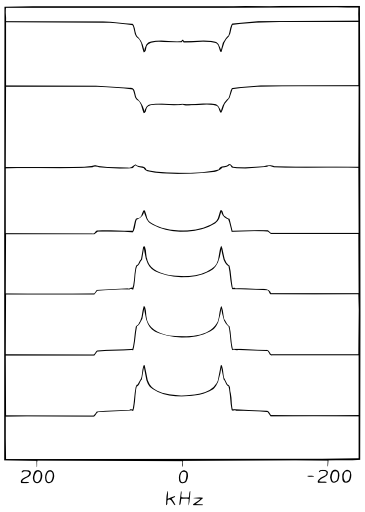

Figure 7. Simulations of partially recovered deuterium line shape data shown in Figure 2A for [d(CGCGAATTC*GCG)]$_2$ labeled with [5,6-$^2H_2$]-2′-deoxycytidine and hydrated to $W = 13$. The reduction of QCC to 170 kHz is simulated as due to a small ampltiude libration of the base about an axis perpendicular to the helix axis ($N = 2$, $\Phi = 6°$, $k = 2.5 \times 10^7$ Hz). To reduce computational time the helix axis model is abbreviated to a slow, three-site jump ($N = 3$, $\Phi = 20°$, $k = 1.25 \times 10^3$ Hz). These modifications of the slow helix motion do not markedly change the line shape.

A. Simulations of Base Motion in dC9. Line shape and relaxation data presented in section 3A indicate that the cytosine base is the least mobile component of dC9. In all respects, line shape and relaxation data obtained for the deuterated cytosine base of dC9 are virtually identical to the data obtained for other base-deuterated DNA oligomers. The dominant trend in the line shape over the hydration range of $W = 0-16.3$, the decay in total spectral intensity with increasing W, can be simulated (Figure 1, right) assuming the oligomer undergoes restricted diffusion about the helix axis, simulated at $W = 12.3$ (Figure 1D) as a multisite jump process ($N = 6$, $k_{helix} = 10^4$ Hz, $\phi_{ij} = 30°$). As the hydration level W increases, the trend in the line shape can be simulated by adjustments of the rotation rate, as shown in Figure 1E ($W = 16.3$, $N = 6$, $k_{helix} = 10^5$ Hz, $\phi_{ij} = 30°$). The slight decrease of QCC_{eff} with increasing W suggests the occurrence of a fast motion, but with very small amplitude. For instance, the reduction of QCC_{eff} from 174 kHz at $W = 0$ to 168 kHz at $W = 10.3$ suggests that any localized motion of the cytosine base cannot exceed 5−10° in amplitude. Line shape simulations suggest that amplitudes of localized motions of the base of dC9 remain small throughout the hydration range of $W = 0-16.3$. Figure 7 shows a simulation of the partially recovered line shape data, shown in Figure 2A, for the base deuterons of dC9 at $W = 13$. The amplitude of local motion of the base is about 6° at a rate of approximately 2.5×10^7 Hz. In summary, deuterium line shape data obtained for the base of dC9 are successfully simulated throughout the hydration range of $W = 0-16$ using a model in which the dominant motion is a uniform rotation of the DNA oligomer about the helix axis, in which rate and amplitude of the uniform rotation varies with hydration level. Simulations of partially relaxed deuterium line shapes indicate the presence of additional motions, probably localized to the cytosine base, that remain small in amplitude throughout the hydration range of study.

B. Simulations of Furanose Ring Motion in dC9. The question of the conformational flexibility of the furanose ring in DNA has received a great deal of attention in the literature. X-ray crystal data indicate that the conformation of the furanose ring characterizes two distinctly different families of nucleic acids: the B form of DNA which is characterized by a rather broad distribution of furanose ring conformations about the C2′-endo conformation and the A form of RNA and DNA which is characterized by a somewhat narrower distribution about C3′-endo.[48] Solution-state NMR studies have probed the conformations of furanose rings in DNA oligomers using proton−proton NOE measurements,[49] relaxation measurements interpreted by model-free methods,[50,51] and proton scalar coupling constants fit to Karplus equations.[9] In particular, proton scalar coupling constants have been analyzed using semiempirical models which assume the furanose ring in DNA interconverts between a small number of pseudorotational conformers. In fact, interconversion between only two conformations, C2′-endo and C3′-endo, is frequently assumed,[9,52,53] although extended treatments have been proposed which incorporate a larger number of "N-like" or "S-like" conformers.[54,55] Theoretical estimates of the barrier to interconversion between C2′-endo and C3′-endo in B form DNA range from 0.5 kcal/mol[56] (a remarkably low barrier, implying virtually free interconversion between furanose ring conformations) to over 2 kcal/mol,[57,58] with a somewhat higher barrier approaching 4 kcal/mol in A form DNA or RNA. Therefore, treating the furanose ring as interconverting between two or a small number of rotational isomers is an approximation at ambient temperature.

In the present study, solid-state deuterium line shape and relaxation data for [2″-^{2}H]deoxycytidine-labeled DNA at $W = 12.3$ are first analyzed in terms of discrete, N-site jump models, where dynamic amplitudes, a priori populations and exchange rates are adjusted to fit experimental data.

B.1. Furanose Rings in DNA at $W = 12.3$. Jumps between Discrete Conformers. Like the corresponding [5,6-$^2H_2$]-2′-deoxycytidine-labeled DNA, the 2″-deuterated DNA dodecamer shows an essentially unaveraged line shape for hydration levels up to $W = 5.5$, which is a hydration level characteristic of A form DNA. The line shape in Figure 3A was simulated assuming the same model of overall molecular rotation about the helix axis ($N = 6$, $k_{helix} = 10^4$ Hz, $\phi_{ij} = 30°$) that was used to simulate the dC9 deuterated base data in Figure 1A. The small reduction of the effective quadrupolar coupling constant of the 2″ deuteron from $QCC_{eff} = 1702$ kHz at $W = 0$ to $QCC_{eff} = 1662$ kHz at $W = 5.5$ may be due to a small amplitude libration (<10°) of the furanose ring about a single equilibrium conformation.

In contrast, the spectrum shown in Figure 3B, corresponding to $W = 12.3$, a hydration level characteristic of B form DNA, is the result of a substantial increase in the amplitude of localized motion at the 2″ deuteron site of dC9. Beginning with a two-site jump ($N = 2$) model and assuming a puckering amplitude

(48) Saenger, W. *Principles of Nucleic Acid Structure*; Springer-Verlag: New York, New York, 1984.
(49) Wuthrich, K. *NMR of Proteins and Nucleic Acids*; John Wiley and Sons: New York, 1986.
(50) Borer, P. N.; LaPlante, S. R.; Kumar, A.; Zanatta, N.; Martin, A.; Hakkinen, A.; Levy, G. C. *Biochemistry* **1994**, *33*, 2441−2450.
(51) Gaudin, G.; Chanteloup, L.; Thuong, N. T.; Lancelot, G. *Magn. Reson. Chem.* **1997**, *35*, 561−565.
(52) Macaya, R.; Wang, E.; Schulze, P.; Sklenar, V.; Feigon, J. *J. Mol. Biol.* **1992**, *225*, 755.
(53) Ven, F. J. M. v. d.; Hilbers, C. W. *Eur. J. Biochem.* **1988**, *178*, 1.
(54) Ulyanov, N. B.; Schmitz, U.; Kumar, A.; James, T. L. *Biophys. J.* **1995**, *68*, 13−24.
(55) Schmitz, U.; Zon, G.; James, T. L. *Biochemistry* **1990**, *29*, 2357.
(56) Levitt, M. *Cold Spring Harbor Symp. Quantum Biol.* **1983**, *47*, 251, 275.
(57) Nilsson, L.; Karplus, M. *J. Comput. Chem.* **1986**, *7*, 591, 616.
(58) Olson, W. K.; Sussman, J. L. *J. Am. Chem. Soc.* **1982**, *104*, 270, 278.

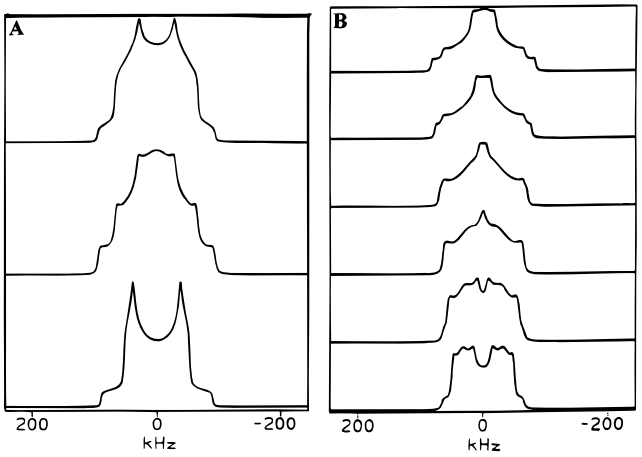

Figure 8. Simulations of the deuterium line shape for [d(CGCGAATTC*GCG)]$_2$ labeled with [2″-^{2}H$_2$]-2′-deoxycytidine and hydrated to $W = 12.3$ using various composite motion models. (A) Localized motion of the furanose ring is portrayed as a two-site exchange ($N = 2$, $\Phi = 38°$, $k = 10^7$ Hz) for which the fractional site populations are $p_1 = 0.8$ and $p_2 = 0.2$. Top: uniform motion about the helix axis is absent. Middle: uniform helix motion is portrayed as ($N = 6$, $\Phi_{ij} = 20°$, $k = 10^4$ Hz). Bottom: uniform helix motion is portrayed as ($N = 6$, $\Phi_{ij} = 60°$, $k = 5 \times 10^6$ Hz). (B) Composite motion models which assume the localized motion of the furanose ring is portrayed as a two-site exchange ($N = 2$, Φ, $k = 10^7$ Hz) for which the fractional site populations are equal $p_1 = p_2$. Φ is varied in increments of 2° from 30° (top) to 40° (bottom). The same uniform helix motion used in A has been applied to the simulations in B.

of $q \approx 0.4$ Å, the angle associated with a discrete jump between the C2′-endo and C3′-endo conformers is about 70°. Given this geometric constraint, the difference in a priori populations and the exchange rate can be adjusted to fit the experimental deuterium line shape data in Figures 3 and 4A. In general, poor fits to experimental data result when disparate a priori populations are assumed, as shown in Figure 8A. Much better simulations of the experimental $W = 12.3$ dC9 DNA line shapes result for two-site jump amplitudes somewhat larger than 70° (half amplitudes in the range of 34−38° appear to fit the data best) and for nearly equal a priori populations (see Figure 8B). Figure 9 shows that, with minor modification of the uniform helix motion, the two-site, equal a priori population model of furanose mobility satisfactorily simulates the partially recovered deuterium line shapes at $W = 12.3$ (see experimental data in Figure 4A), although the line shapes near the T_1 null are not well simulated. The simulations in Figure 9 assume a jump half angle of 38−40° for the furanose ring and a jump rate on the order of 10^7 Hz.

To further test the hypothesis that averaging of the deuterium line shape at hydration levels $W \geq 12.3$ is due to at least two motional processes, corresponding to a localized motion of the furanose ring and a uniform motion of the oligomer, the line shape of the 2” deuteron of dC9 was studied at temperatures low enough to almost completely freeze out uniform motion of the oligomer. Figure 10A shows the experimental line shape for the 2” deuteron of dC9 in DNA hydrated to $W = 13.6$ and cooled to a temperature of $T = 198$ K. The simulated line shape in Figure 10B assumes that uniform motion of the dodecamer is absent and that the localized motion of the furanose ring is described, as before, by a discrete two-site jump with half angle 38° and a rate of 10^6 Hz.

Two-site exchange is the simplest possible model for furanose ring motion, so models that involve exchange between three or more discrete furanose ring conformers have also been investigated. Multisite jump models involve a markedly larger parameter set than the two site exchange model. For an N-site jump model, N sets of Euler angles, each set defining the orientation of the EFG tensor in each conformer, must be specified. Therefore, for an arbitrary N site model the parameter set consists of N resonance frequencies (specified by N sets of Euler angles), N a priori populations, and the site i residence time τ, assumed to be equal for all sites.

The equilibrium sites occupied by deuterons attached to carbon atoms in the furanose ring of dC9 are assumed be located along arcs, defined by the motion of the C2′−D2″ bond as the D−C−C−H torsion angle changes due to changes in the puckering of the furanose ring. To further simplify the problem we assume that jumps occur only between “nearest neighbor” sites. For nearest neighbor exchange and equal a priori site

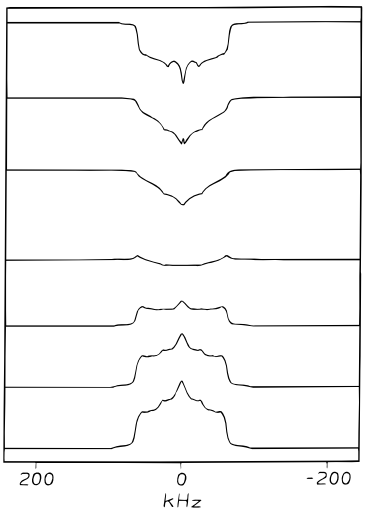

Figure 9. Simulations of partially recovered deuterium line shape data shown in Figure 4A for [d(CGCGAATTC*GCG)]$_2$ labeled with [2″-^{2}H$_2$]-2′-deoxycytidine and hydrated to $W = 12.3$. The localized motion of the furnaose ring is simulated as a two-site exchange with equal site populations ($N = 2$, $\Phi = 38°$, $k = 10^7$ Hz). To reduce computational time the helix axis model is abbreviated to a slow, three-site jump ($N = 3$, $\Phi = 20°$, $k = 1.25 \times 10^3$ Hz).

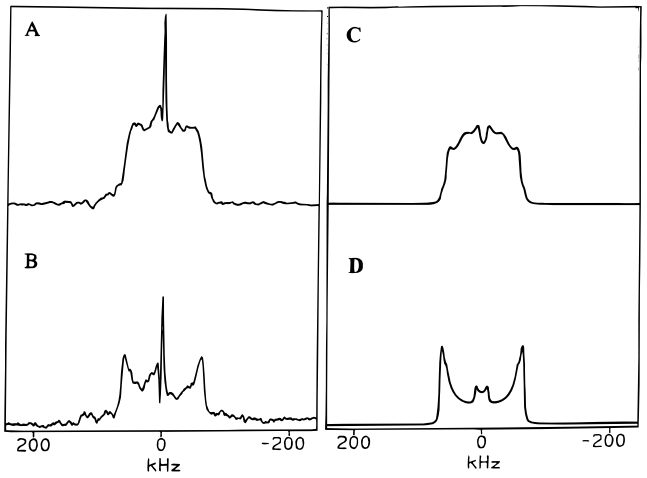

Figure 10. (A) Deuterium solid-state NMR spectrum of [d(CGCGAATTC*GCG)]$_2$ labeled with [2″-^{2}H$_2$]-2′-deoxycytidine, hydrated to $W = 13.6$, and cooled to a temperature of $T = 198$K. (B) Simulation of the data in A assuming absence of uniform motion of the oligomer. The motion of the C−D bond is portrayed as ($N = 2$, $\Phi = 38°$, $k = 10^6$ Hz).

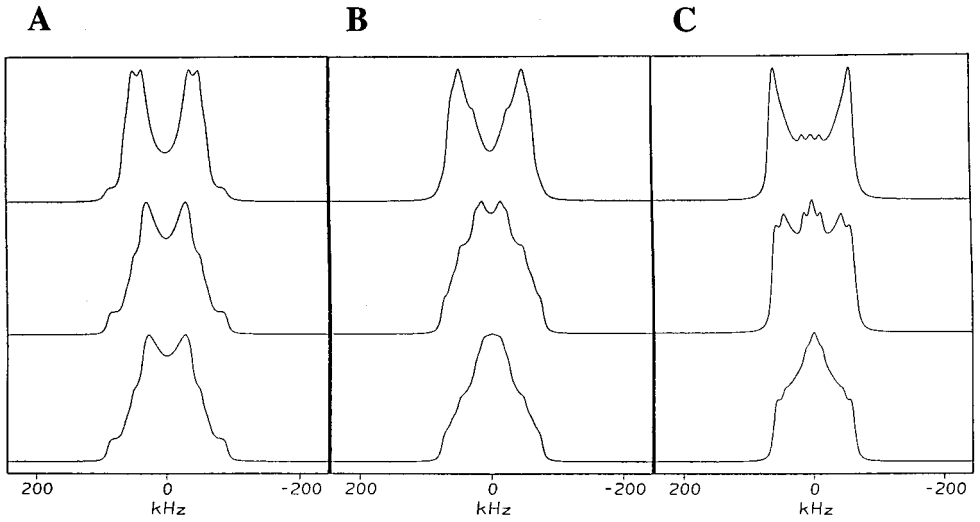

Figure 11. The localized motion of the furanose ring approximated as a four-site libration with half amplitudes 38° and 5°. Site 1 corresponds to the C2′−D2″ bond oriented 22° to the helix axis. Rotation about the helix axis occurs at a rate of 10^5 Hz. Site 3 is oriented 76° from site 1. Sites 2 and 4 are located at intervening positions. (A) Equal a priori site populations. Top: $k = 10^6$ Hz. Middle: $k = 10^7$ Hz. Bottom: $k = 10^8$ Hz. (B) Unequal site population: site 1 = 0.35, site 2 = 0.15, site 3 = 0.35, site 4 = 0.15. Top: $k = 10^6$ Hz. Middle: $k = 10^7$ Hz. Bottom: $k = 10^8$ Hz. (C) Unequal site populations: site 1 = 0.45, site 2 = 0.05, site 3 = 0.45, site 4 = 0.05. Top: $k = 10^6$ Hz. Middle: $k = 10^7$ Hz. Bottom: $k = 10^8$ Hz.

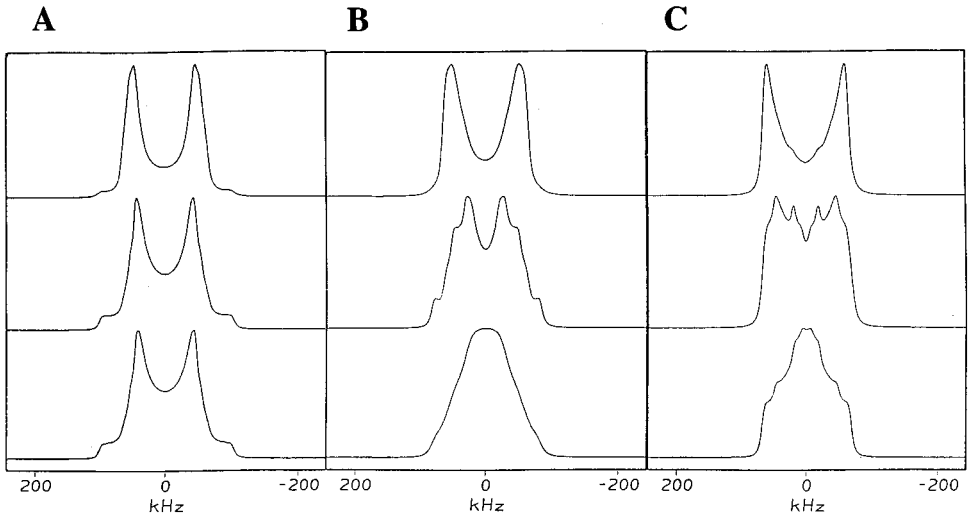

Figure 12. Localized motion of the furanose ring is approximated as an exchange between six sites located on an arc with site 1 corresponding to the C2′−D2″ bond oriented 22° to the helix axis and site 4 oriented at 76° from site 1. Sites 2, 3, 5, and 6 are located at intervening positions between sites 1 and 4. Rotation about the helix axis occurs at a rate of 10^5 Hz. (A) Equal a priori probabilities with nearest neighbor jumps occurring at 10^6 Hz. (top), 10^7 Hz. (middle), and 10^8 Hz. (bottom). (B) Sites 1 and 4 with fractional populations of 0.3 each and all interveneing sites with fractional populations of 0.10 each. The dynamics are modeled as nearest neighbor jumps occurring at 10^6 Hz. (top), 10^7 Hz. (middle), and 10^8 Hz. (bottom). (C) Sites 1 and 4 with fractional populations of 0.40 each and the intervening sites with populations of 0.05 each. The dynamics are modeled as nearest neighbor jumps occurring at 10^6 Hz. (top), 10^7 Hz. (middle), and 10^8 Hz. (bottom).

populations, the R matrix has the form

$$\kappa \begin{pmatrix} -2 & 1 & 0 & .. & 1 \\ 1 & -2 & 1 & .. & 0 \\ 0 & & & & .. \\ .. & .. & 1 & -2 & 1 \\ 1 & 0 & .. & 1 & -2 \end{pmatrix} \tag{7}$$

where $\kappa = 1/\tau_c$.

Despite the size of the parameter set, which is large even with the constraints described above, distinct trends in the deuterium line shape can be identified. Figure 11 shows a series of simulated line shapes obtained for four-site jump models as a function of a priori site population and exchange rate. Models that assume exchanges between four sites with equal a priori populations, shown in Figure 11A, generally result in narrow powder patterns that do not resemble the experimental line shapes observed in the hydration range of $W > 5.5$. Simulated four-site exchange line shapes which fit deuterium line shapes at $W > 5.5$ at least as well as two-site jumps are obtained as the a priori populations of intervening sites are decreased and the populations of sites at $\theta = 38°$, $\phi = 0, 180°$ are increased (see Figure 11B,C). A similar trend is observed for six- and eight-site jump models (see Figure 12). We conclude that if the furanose ring of dC9 exchanges between more than two pseudorotational conformers, the a priori populations of the additional sites are at most a 10−20% effect.

B.2. Simulation of Deuterium NMR Data for Furanose Rings in DNA at $W > 12.3$. Simulation of deuterium line shapes at higher levels of hydration, i.e., $W > 16.3$, is complicated by extensive averaging from uniform rotation of

the DNA oligomer that increases in amplitude and rate as the hydration sites on DNA saturate and water fills the space between DNA oligomers. The separation of the time scales of the uniform motion and the localized internal motions of the oligomer diminishes for hydration levels $W > 20$, where the rate of uniform motion approaches or exceeds 10^6 Hz.[30] In addition, for $W = 22-25$ and higher, magnetic alignment of DNA oligomers occurs.[60]

Numerous NMR studies of base-, sugar-, and backbone-deuterated DNA dodecamers indicate that at high hydration levels i.e., $W > 20$, uniform rotation of the DNA oligomer about the helix axis can be simulated by simply increasing the amplitude and rate of the motion (i.e., $N = 6$, $k_{helix} > 10^6$ Hz, $\phi_{ij} = 60°$). A minor component arises from restricted rotation of the oligomer about an axis perpendicular to the helix axis and may also occur for $W > 22$. Thus, as mentioned above, the rate and amplitude of uniform modes of rotation are not treated as freely adjusted parameters for $W > 22$ in the current study, but rather are set to values determined from a large number of deuterated dodecamers.

The second major effect at high hydration levels, magnetic alignment of DNA, has been studied by X-ray diffraction and optical methods,[61,62] high-resolution NMR,[63] and solid-state NMR.[60,64] At high levels of hydration, DNA forms a cholesteric phase, where the helix axis is inclined at an angle $\beta \approx 90°$ to the magnetic field direction. In studies of magnetically aligned cholesteric liquid crystals, the deuterium line shape $I(\omega)$ has been simulated assuming a superposition of various β orientations characterized by a weighting function $f(\beta)$[65]

$$I(\omega) = \int I(\omega,\beta)\, f(\beta)\, \sin(\beta)\, d\beta \qquad (8)$$

Various forms for $f(\beta)$ are available but a Gaussian distribution has been found to give the best fit to experimental line shapes

$$f(\omega) = (P/\sigma\sqrt{2\pi})e^{-(\beta-\beta_o)^2/2\sigma^2} + (1 - P) \qquad (9)$$

where P is the fraction of the sample in oriented domains, β_o is the mean angle of alignment, and σ is the standard deviation of the Gaussian distribution. Deuterium NMR studies of selectively deuterated DNA dodecamers indicate good fits to experimental line shapes over a range of temperatures for $P = 0.7$, $\beta_o = 90°$, and $\sigma \approx 15°$[33]. The results of independent deuterium NMR studies of the cholesteric ordering of DNA dodecamers ($P = 0.7$, $\beta_o = 90°$, and $\sigma \approx 15°$) and the rates and amplitudes of uniform motion similarly derived by independent studies of DNA dodecamers at high hydration levels ($N = 6$, $k_{helix} = 5 \times 10^6$ Hz, $\phi_{ij} = 60°$) were combined with the model of furanose motion derived at lower hydration levels for [2″-^{2}H]-2′-deoxycytidine-labeled DNA ($N = 2$, $k = 10^7$ Hz, $\theta = 38-40°$) to produce the simulated line shape in Figure 3F. Agreement with the experimental line shape in Figure 3C is excellent.

Thus far we have considered the nature of internal motions of the furanose ring of dC9 for rates spanning the range of 10^4-10^8 s^{-1}. Analysis of the amplitude of the spin alignment echo can probe ultraslow motions which occur at rates less than 10^4 s^{-1}. A simple N-site exchange model can be applied to the spin alignment echo data for the furanose ring of of dC9, shown in Figure 4B. In the limit $\tau_1 \gg 1/\omega_Q$ and $\tau_2 \gg \tau_c$, the correlation function for spin alignment is $F(\tau_1, \tau_2) = \Sigma_{i=1}^{-} P_i^2$, where P_i is the fractional population of site i. Using this limiting form for the spin alignment correlation function, the spin alignment echo amplitude is given by[46]

$$S(\tau_2) = (1 - f)\exp\left(-\frac{\tau_2}{\tau_c} - \frac{\tau_2}{\tau_{1Q}}\right) + f\exp\left(-\frac{\tau_2}{\tau_{1Q}}\right) \qquad (10)$$

where $f = \Sigma_{i=1}^{-} P_i^2$. For a two-site exchange, $N = 2$ and f has a minimum value of 0.5. Making the order-of-magnitude approximation that $\tau_c = 1$ ms and given $T_{1Q} = 0.025$ s, we find $f = 0.90$. A similar result was obtained for the furanose ring of thymidine by Hiyama et al.[46]

C. Simulations of Backbone Motions at dC9. Although the data for the 5′/5″ deuterons of dC9, shown in Figure 6A, possess insufficient signal-to-noise to enable a detailed line shape analysis, some useful information can be obtained. The line shape is motionally narrowed to the extent that QCC_{eff} cannot exceed 60 kHz at $W = 10.1$. The effective asymmetry parameter η_{eff} cannot be determined accurately but it is small and certainly less than 0.1. Because limited signal-to-noise prevents an accurate measurement of η_{eff}, discussion of the line shape will be confined mainly to the reduction factor $\Lambda = QCC_{eff}/QCC_{static}$ which, unlike the order parameter S, does not involve η_{eff}. Assuming $QCC_{static} = 175$ kHz, the 5′/5″ deuteron line shape for dC9 reflects a reduction factor of $\Lambda = QCC_{eff}/QCC_{static} \approx 0.34$. A very different result is obtained for the 5′/5″ deuterons of dT7 and dT8 in the same dodecamer where, at $W = 10.5$, $QCC_{eff} = 15 \pm 22$ kHz, i.e., $\Lambda = 0.87$. In fact, even at hydration levels as high as $W = 21$, QCC_{eff} never decreases to less than 143 kHz and therefore is never less than 0.82 at the dT7 and dT8 backbone sites. Previous deuterium NMR studies of the dT7 and dT8 backbone sites analyzed deuterium solid-state line shapes in terms of three motional models: (1) diffusion of the C5′−D bond in a cone defined by half-angle θ; (2) a four site libration defined by half-angles θ and ϕ; (3) a three-site trans−gauche isomerization.

For the cone diffusion model, the reduction factor is given by

$$\Lambda = {}^1/_2 \cos\theta(1 + \cos\theta) \qquad (11)$$

where θ is the cone half angle. For the cone diffusion model, the effective asymmetry parameter is zero. From Figure 13A, a reduction parameter of $\Lambda \approx 0.34$ would require a half-angle θ approaching 60°.

A somewhat more elaborate model would admit a biaxial character to the motion of the 5′ methylene group. The simplest such model is a four site jump model, for which application of eqs 4a and 4b yields eq 12, where $\xi_{ij}^{\pm} = p_i^{eq} \pm p_j^{eq}$. Figure

$$\bar{V} = -\frac{eq}{2}\begin{pmatrix} \xi_{34}^{+} + \xi_{12}^{+}(1-3\sin^2\theta) & 0 & \frac{3}{2}\xi_{12}^{-}\sin 2\theta \\ 0 & \xi_{12}^{+} + \xi_{34}^{+}(1-3\sin^2\theta) & -\frac{3}{2}\xi_{34}^{-}\sin 2\phi \\ \frac{3}{2}\xi_{12}^{-}\sin 2\theta & -\frac{3}{2}\xi_{34}^{-}\sin 2\phi & \xi_{12}^{+}(1-3\cos^2\theta) + \xi_{34}^{+}(1-3\cos^2\phi) \end{pmatrix} \qquad (12)$$

13B is a contour plot of the reduction factor and η_{eff} as functions of the half-angles θ and ϕ for the case of equal site populations.

(59) Nadler, W.; Schulten, K. *J. Chem. Phys.* **1986**, *84*, 4015.
(60) Alam, T. M.; Drobny, G. P. *J. Chem. Phys.* **1990**, *92*, 6840−6846.
(61) Iizuka, E. *Polym. J.* **1983**, *15*, 525.
(62) Skuridin, S.; Badaev, N.; Dembo, A.; Lortkipanidze, G.; Yevdokimov, Y. *Liq. Cryst.* **1988**, *3*, 51.
(63) Rill, R. L.; Hillard, P. R.; Levy, G. C. *J. Biol. Chem.* **1983**, *258*, 250.
(64) Brandes, R.; Kearns, D. R. *Biochemistry* **1986**, *25*, 5890.
(65) Luz, Z.; Poupko, R.; Samulski, E. T. *J. Chem. Phys.* **1981**, *74*, 5825.

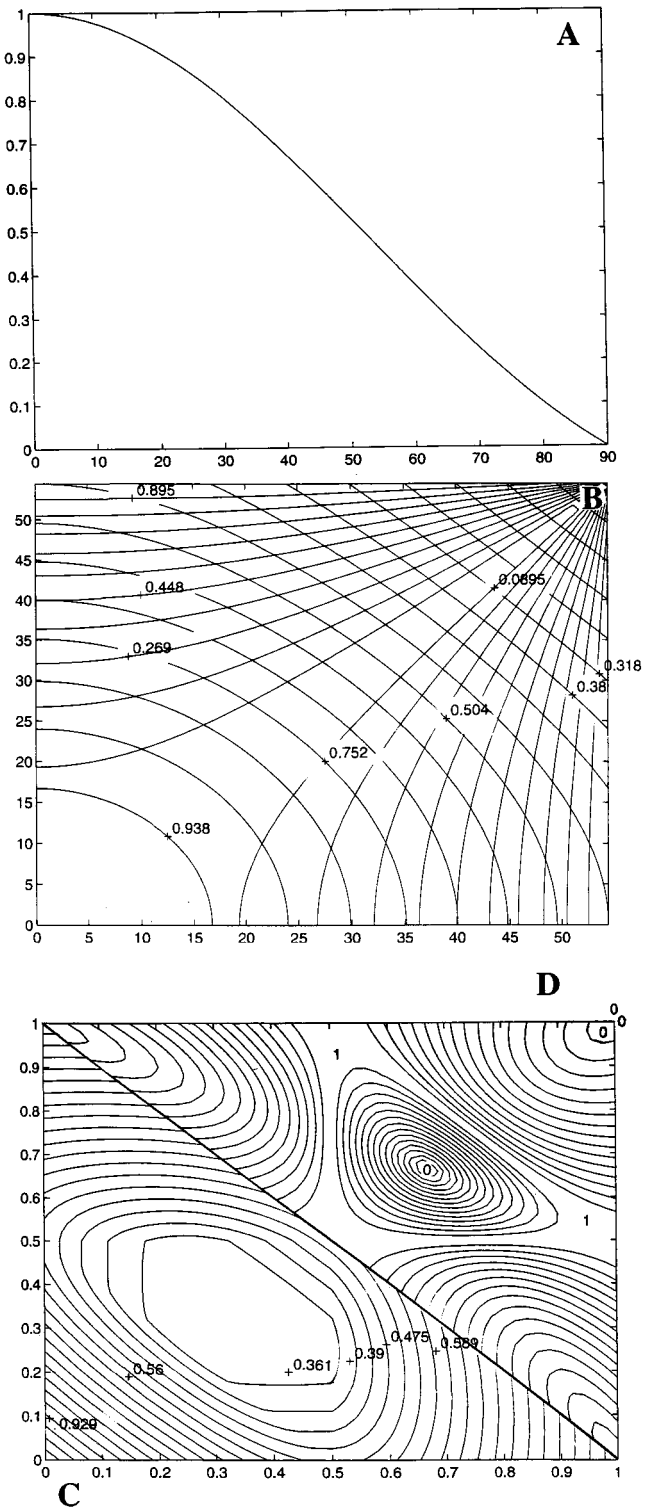

Figure 13. Reduction factor calculated for various models of the motion of the 5′ methylene group of dC9: (A) For a diffusion-in-a-cone model plotted as a function of cone-half angle. The effective asymmetry parameter is zero for this model. (B) Contour plot of as a function of jump half angles for a biaxial four-site exchange (eq 18). Lines of equal appear as circular patterns of varying radii. The effective asymmetry parameter is also plotted assuming the convention stated in eq 2, where contours converging at higher amplitudes are lines of equal. (C) Plotted as a function of equilibrium populations p_1 and p_2 ($p_1 + p_2 < 1$) for a rotational isomeric state (RIS) model (eq 19). (D) The effective asymmetry parameter for the RIS model plotted as a function of p_1 and p_2.

Even in the absence of accurate information on the effective asymmetry, a reduction factor of 0.34 requires that the root-mean-square half-angle rms$(\theta,\phi) = \sqrt{(\theta^2+\phi^2)/2} \approx 40-41°$, if the effective asymmetry parameter does not exceed 0.1.

A rotational isomeric state (RIS) model has been used to describe the motion of the phosphodiester backbone of DNA[48,66] where the rotational axis is coincident with the C4′−C5′ bond and the torsional angle γ fluctuates between gauche−gauche (+sc), gauche−trans (sp), and trans−gauche (−sc) with unequal site probabilities. Using eqs 2a and 2b, with $\phi_1 = 0°$, $\phi_2 = 120°$, and $\phi_3 = 240°$, yields eq 13, where θ is the angle between the rotational axis and the C5′−H bond, $\xi_{jk}^{\pm} = p_j^{eq} \pm p_k^{eq}$, and the fractional site populations satisfy $p_1^{eq} + p_2^{eq} + p_3^{eq} = 1$. A plot of the reduction factor Λ as a function of the equilibrium probabilities is shown in Figure 13C. For the 5/5″ deuterons of dT7 and dT8, a RIS model fits the data only at low hydration levels ($W = 4.8$). In that case the reduction factor was much larger, i.e., $\Lambda = 0.94$ and $\eta_{eff} = 0.06$ so that $p_1 = 0.94$, $p_2 = 0.05$, and $p_3 = 001$. Figure 13C shows that such a population distribution cannot produce the reduction factor observed at dC9, and to achieve a reduction factor of 0.34, substantial populations at all three sites must occur. Specifically, the reduction factor surface is a broad minimum for, $\Lambda < 0.39$, and for $\Lambda \approx 0.34$, both p_1 and p_2 must lie in the range of 0.3−0.4. The effective asymmetry parameter is shown in Figure 13D as a function of p_1 and p_2. In the range of $p_1 = 0.3-0.4$ and $p_2 = 0.3-0.4$, the effective asymmetry parameter surface is a steep minimum centered about zero.

5. Discussion

Much discussion has appeared in the literature regarding the exact nature of the internal motions of DNA in solution.[33−35,78−89] The complexity of the problem is in part a result of the

(66) Yathindra, N.; Sundaralingam, M. *Biopolymers* **1973**, *12*, 297, 314.
(67) Calladine, C. R. *J. Mol. Biol.* **1982**, *166*, 343−352.
(68) Dickerson, R. E.; Drew, H. R. *Proc. Nat. Acad. Sci. U.S.A.* **1981**, *78*, 7318−7322.
(69) Trifonov, E. N. *Nucleic Acids Res.* **1980**, *8*, 4041, 4053.
(70) Main chain conformation angles are defined as $P\overset{\alpha}{-}O5'\overset{\beta}{-}C5'\overset{\gamma}{-}C4'\overset{\delta}{-}C3'\overset{\epsilon}{-}O3'\overset{\zeta}{-}P$.
(71) Dickerson, R. E. *J. Mol. Biol.* **1983**, *166*, 419−441.
(72) Herzyk, P.; Rabczenko, A. *J. Chem. Soc., Perkin Trans. 2* **1985**, 1925−1930.
(73) Marzec, C. J.; Day, L. A. *J. Biomolec. Struct. Dyn.* **1993**, *10*, 1091−1123.
(74) Rudnicki, W. R.; Lesyng, B.; Harvey, S. C. *Biopolymers* **1994**, *34*, 383−392.
(75) Altona, C.; Sundaralingam, M. *J. Am. Chem. Soc.* **1972**, *94*, 8205−8212.
(76) Dickerson, R. E.; Kopka, M. L.; Drew, H. R. In *Structural Correlations in Biology*; Dickerson, R. E., Kopka, M. L., Drew, H. R., Eds.; Adenine Press: New York, 1982.
(77) Dumais, J. J. In *Molecular Motion in the Backbone of Synthetic Oligonucleotides: A Phosphorus NMR Study*; Dumais, J. J., Ed.; University of Washington: Seattle, WA, 1992.
(78) Allison, S. A.; Shibata, J. H.; Wilcoxon, J.; Schurr, J. M. *Biopolymers* **1982**, *21*, 729−762.
(79) Assa-Munt, N.; Granot, J.; Behling, R. W.; Kearns, D. R. *Biochemistry* **1984**, *23*, 944−955.
(80) Bendel, P.; Lamb, O.; James, T. L. *J. Am. Chem. Soc.* **1982**, *104*, 6748−6754.
(81) Bendel, P.; James, T. L. *Proc. Natl. Acad. Sci. U.S.A.* **1983**, *80*, 3284−3286.
(82) Bolton, P. H.; James, T. L. *J. Am. Chem. Soc.* **1980**, *102*, 25, 31.
(83) Davanloo, P.; Armitage, I. M.; Crothers, D. M. *Biopolymers* **1979**, *18*, 663−680.
(84) Early, T. A.; Kearns, D. R.; Hillen, W.; Wells, R. D. *Biochemisty* **1981**, *20*, 3764−3769.
(85) Georghiou, S.; T, D. B.; Philippetis, A.; Beechem, J. M. *Biophys. J.* **1996**, *70*, 1909−1922.
(86) Hogan, M. E.; Jardetsky, O. *Biochemistry* **1980**, *19*, 2079−2085.
(87) Keepers, J. W.; James, T. L. *J. Am. Chem. Soc.* **1982**, *104*, 929−762.

$$\bar{V} = -\frac{eq}{2}\begin{pmatrix} p_1^{eq}(1-3\sin^2\theta)+\xi_{23}^{+}(1-{}^3/_4\sin^2\theta) & -\xi_{23}^{-}\frac{3\sqrt{3}}{4}\sin^2\theta & p_1^{eq}\,{}^3/_2\sin 2\theta-\xi_{23}^{+}\sin 2\theta \\ -\xi_{23}^{-}\frac{3\sqrt{3}}{4}\sin^2\theta & p_1^{eq}+\xi_{23}^{+}(1-{}^9/_4\sin^2\theta) & -\xi_{23}^{-}\frac{3\sqrt{3}}{4}\sin 2\theta \\ p_1^{eq}\,{}^3/_2\sin 2\theta-\xi_{23}^{+}\sin 2\theta & -\xi_{23}^{-}\frac{3\sqrt{3}}{4}\sin 2\theta & 1-3\cos^2\theta \end{pmatrix} \quad (13)$$

composite nature of the dynamics of DNA. At issue is how in general to accurately distinguish collective motions of the helix and strictly localized motions of the individual nucleotides. Under the sample conditions used in our solid-state NMR study, much of the uncertainty in data interpretation has been removed. We have found that in the hydration range of $W = 10-12.6$, comparable to the level of hydration in a B form DNA crystal, large amplitude motions of the furanose ring and phosphodiester backbone at the C9pG10 step occur at rates separated by about 3 orders of magnitude from overall motions of the helix in the hydrated solid state. The result is a relatively simple situation, where localized internal motions at a CpG step in B form DNA occur at appropriate time scales and with sufficient amplitude to produce intermediate-regime averaging of the deuterium line shapes, while the effects of very slow overall motions on the line shape are slight. Under such conditions, some features of the localized motions of the C9pG10 step can be clarified.

In the hydration range of $W = 5.5-10$, within which DNA undergoes a transition from the A form to the B form, the deuterium NMR line shapes for the 2″ and 5′/5″ deuterons of dC9 change from essentially rigid Pake doublets to motionally averaged powder patterns. Mobility of the CpG step is therefore a feature of B form DNA and is absent or greatly reduced in amplitude when the molecule is in the A form. Regardless of the specific model used to interpret the deuterium line shape of the dC9 furanose ring in B form DNA, we are led to conclude that the C9pG10 step cannot be adequately described by a single equilibrium structure, viewed as only slightly perturbed by motion. On the contrary, motions strongly perturb a great portion of the C9pG10 step, and it is clear that the flexible furanose ring of dC9 intersects a locally flexible portion of the phosphodiester backbone. In addition our line shape simulations enable us to exclude certain models of furanose ring motion from consideration. For example, free angular diffusion of the furanose C2′−D2″ bond within a well does not fit the deuterium line shape data at any point in the hydration series. Our line shape simulations do support the view that a mobile furanose ring diffuses in a double well potential, which we have approximated by a two-site jump, but we do not find that the a priori populations of the minimum energy conformers of the furanose ring of dC9 differ markedly. Therefore, we would not characterize the motion of the dC9 furanose ring as an exchange between a dominant "S-like" conformer and a minor "N-like" confomer.

Another significant result of our study is that the rate of localized, large amplitude motion of the furanose ring of dC9 can be confined to the range of 10^7-10^8 Hz at ambient temperature for hydration levels up to $W = 22$. If the large amplitude motion of the furanose ring of dC9 occurs at similar rates under solution conditions, the time scale of this motion is actually longer than the time scale of the rotational diffusion of the dodecamer under solution conditions.

Dynamics at the C9pG10 step are possibly of functional relevance, because this region of the DNA dodecamer is involved in a number of sequence-specific interactions with the EcoRI restriction enzyme.[94−96] Structural deviations at the C9pG10 step are thought to contribute to sequence-specific recognition in this system, and specific models have been proposed to explain this variability.[67−69] For example, steric clash between G10 and G4 is believed to result in a number of modifications of the double helix including reduction of the propeller twist, opening of the roll angle θ_R, reduction of the local twist angle between base pairs, and lateral shift of the G−C base pair. To preserve a phosphate−phosphate distance of 6.68 Å, lateral shift of the dC9-dG4 base pair is accompanied by an increase in the δ torsion angle[70] for a purine or a decrease in δ for a pyrimidine, where the sugar−base−sugar−base assembly is considered a functional unit, which swivels at the glycosyl bonds but has few other internal degrees of freedom.[2,68,71] A segmented rigid body analysis of the X-ray data[17] also indicates the base and furanose rings in [d(CGCGAATTCGCG]$_2$ move as rigid assemblies.

The results of this solid-state NMR study indicate that once hydration levels characteristic of B form DNA are achieved, large amplitude motions of the furanose rings and helix backbone occur in regions of the DNA dodecamer (i.e., the C9pG10 step) that X-ray data and high-resolution NMR data indicate are statically modified from B form. In addition, preliminary solid-state NMR line shape data indicate that the furanose ring of dC3 is also highly mobile under similar experimental conditions.[47] As a result, we conclude that within the CpG steps adjacent to the restriction enzyme cutting site, dynamic modulations are so marked that many of the torsion angles within the pyrimidine nucleotides simply cannot be assigned single, discrete values. For the furanose ring of dC9, we find the C2′−D2″ bond moves within 10 ns through a full arc of between 76° and 80°, which is somewhat larger than the amplitude expected for an interconversion from C2′-endo to C3′-endo. Regardless of whether this motion is viewed as an exchange between 2, 4, or more discrete sites, line shape simulations indicate no single furanose ring conformer possesses a dominant a priori probability. Because the δ torsion angle and furanose ring puckering are interdependent,[48,56,76] a motion which changes the sugar pucker of dC9 might be expected to affect this torsion angle as well. For example, if the furanose of dC9 ring exchanges between C2′-endo to C3′-endo, δ changes from 144° to 82°, or a total angular change of over 60°. In addition, the fact that the C5′/5″ deuterons display large amplitude mobility in dC9 suggests the possibility of a coupling to the motion of the furanose ring. Our data do not allow us to uniquely identify the detailed nature of motion of the C5′

(88) Langowski, J.; Fujimoto, B. S.; Wemmer, D. E.; Benight, A. S.; Drobny, G.; Shibata, J. H.; Schurr, J. M. *Biopolymers* **1985**, *24*, 1023−1056.
(89) Schurr, J. M.; Fujimoto, B. S. *Biopolymers* **1988**, *27*, 1543, 1569.
(90) Lipari, G.; Szabo, A. *J. Am. Chem. Soc*. **1982**, *104*, 4559.
(91) Eimer, W.; Williamson, J. R.; Boxer, S. G.; R. Pecora *Biochemistry* **1990**, *29*, 799−811.
(92) Schurr, J. M.; Babcock, H. P.; Fujimoto, B. S. *J. Magn. Reson.* **1994**, *B105*, 211−224.
(93) Withka, J. M.; Swaminathan, S.; Bolton, P. H. *J. Magn. Reson.* **1990**, *89*, 386-390.
(94) Kim, Y.; Grable, J. C.; Love, R.; Greene, P. J.; Rosenberg, J. M. *Science* **1990**, *249*, 1307.
(95) McClarin, J. A.; Frederick, C. A.; Wang, B.-C.; Greene, P.; Boyer, H. W.; Grable, J.; Rosenberg, J. M. *Science* **1986**, *234*, 1526−1541.
(96) Lesser, D. R.; Kurpiewski, M. R.; Jen-Jacobson, L. *Science* **1990**, *250*, 776−786.

methylene group in dC9 but certain types of motions at the 5′ methylene are expected to be more strongly coupled to the furanose ring than others. For example, on the basis of 127 nucleoside/nucleotide structures, Tomita et al.[97] found no evidence of a statistical correlation between the pucker of the furanose ring and the γ torsion angle. Thus, if the motion of the 5′ methylele deuterons in dC9 is an interconversion between rotational isomers of the C4′-C5′ bond, the motion changes γ and a coupling to the puckering motion of the furanose ring of dC9 would not be expected. On the other hand, the averaging of the deuterium NMR powder pattern of the 5′/5″ deuterons may also be the result of a large amplitude libration of the C4′-C5′ bond, which might occur as a result of a fluctuation of the δ torsion angle. In summary, within dC9 and probably within dC3 as well, neither the furanose puckering, the δ torsion angle, nor possibly the γ torsion angles can be assigned single, discrete values but rather fluctuate at rates on the order of 10^7 Hz. In addition, spin alignment experiments detect motions of the furanose ring of dC9 at rates on the order of 10^3 Hz.

Our solid-state NMR data are in qualitative agreement with the results of some high-resolution NMR studies. For example, Bax and Lerner[9] concluded from an analysis of proton *J*-couplings that the furanose rings of dC3 and dC9 in [d(CGCGAATTCGCG)]$_2$ must exist in a number of conformations, although they assigned a dominant equilibrium distribution to an S-like conformer. A high-resolution ^{31}P NMR study of [d(CGCGAATTCGCG)]$_2$ by Ott and Eckstein[8] reported that the transition frequencies of the phosphate residues at positions 3 and 9 occur at lower fields than expected, which the authors suggested indicates a "break in conformation" at these positions. Localized mobility of the phosphodiester backbone is also supported by a solid-state ^{31}P study of the same dodecamer which observed the occurrence of two powder patterns at $W = 10$ and above: a motionally narrowed pattern and a broader component.[77] Finally, a recent high-resolution NMR study reports pronounced localized dynamics at a TpA step in the T3A3 cleavage site of the AhaIII and PmeI restriction sequences,[98] indicating that large amplitude dynamics may be a component of sequence-specific recognition in those systems as well.

6. Conclusions

Regardless of the specific details of the models used to simulate the line shapes of deuterons located in dC9 (and in dC3), we can conclude that the CpG steps located near the restriction enzyme cutting site are substantially affected by internal motions of the pyrimidine furanose rings and the phosphodiester backbone. Deuterium NMR analysis of the mobility of the furanose rings and phosphodiester backbone are being extended to most of the remaining regions of the restriction enzyme binding site and when completed will provide a better view of the nature of localized dynamics throughout this DNA dodecamer. Work presently in progress also includes determining the degree to which variations in local sequence influence localized dynamics and the degree to which local motions are perturbed by chemical alterations such as base methylation. Finally, the question of whether the dynamics reported in this study occur in crystalline DNA is being addressed with solid-state deuterium NMR to the study crystals of selectively deuterated DNA.

Acknowledgment. G.P.D. thanks Professors R.R. Vold and R.L. Vold for providing copies of MXQET and MXET1 and is additionally grateful to Dr. Joanna Long, Professors J. M. Schurr, B. H. Robinson, and B. R. Reid for many helpful discussions. This research was supported by NIH Program Project Grant GM32681. M.E.H. acknowledges support from NIH Molecular Biophysics Training Grant GM08268.

JA971266H

(97) Kitahura, K., Wakahara, A., Mizuno, H., Baba, Y., and Tomita, K.-I. *J. Am. Chem. Soc.* **1981**, *103*, 3899−3904.

(98) Kennedy, M. A.; Nuutero, S. T.; Davis, J. T.; Drobny, G. P.; Reid, B. R. *Biochemistry* **1993**, *32*, 8022−8035.